ACS OMEGA

http://pubs.acs.org/journal/acsodf

Article

Hydrogenation Effect on Interlayer Coupling and Magneto-Transport Properties of Pd/Co/Mg/Fe Multilayers

Li-Jie Liaw, Zi-Qi Liu, Po-Wei Chen, Shi-Yu Liu, Alltrin Dhanarajagopal, Fang-Yuh Lo, Jhen-Yong Hong,* and Wen-Chin Lin*

Cite This: *ACS Omega* 2023, 8, 26948−26954

Read Online

ACCESS | Metrics & More | Article Recommendations | Supporting Information

ABSTRACT: Hydrogenation-induced modification of magnetic properties has been widely studied. A Mg spacer layer with high hydrogen storage stability was clamped in a Pd/Co/Mg/Fe multilayer structure to enhance its hydrogen storage stability and explore the structure's magneto-transport properties. After 1 bar hydrogen exposure, the formation of a stable MgH_2 phase was demonstrated in an ambient environment at room temperature through X-ray diffraction. Lower magnetic coupling and enhanced magnetoresistance, compared to those of the as-grown sample, were observed using the longitudinal magneto-optical Kerr effect and a four-probe measurement. In this study, the hydrogenation stability of ferromagnetic multilayers was improved, and the concept of a hydrogenation-based spintronic device was developed.

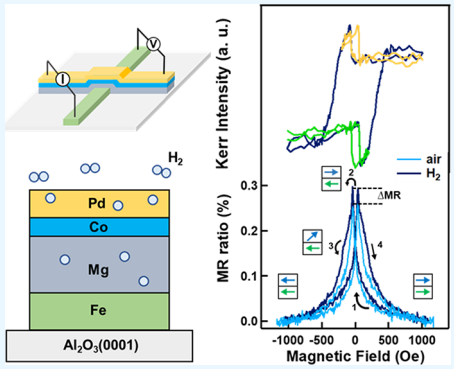

INTRODUCTION

Magnetism and spintronics have been studied for several decades. Magnetic storage and magnetic random-access memory devices based on the giant magnetoresistance (MR) effect and tunneling MR have caused substantial evolution in the storage industry.[1−7] The use of different alloys or layer thicknesses is usually effective in controlling magnetic properties such as coercivity (H_c) and magnetic anisotropy. However, once a device has been fabricated, changing its magnetic properties, including enhancing its MR or altering the magnetic easy axis or H_c, is difficult.[8,9] Hydrogenated magnetism has been extensively studied for decades.[10−12] The effect of hydrogen on magnetic properties such as easy axis rotation, H_c modification, and magnetic anisotropy control has been extensively examined.[13] Pd is a popular hydrogen storage material because of the highly catalytic H_2 dissociation of the Pd−H system at room temperature (RT).[14] Because of the high hydrogen sensitivity[15,16] and high magnetic susceptibility of a Pd system, Pd hydride can effectively induce electron exchange in magnetic materials and indirectly affect their magnetism.[17−19] However, a Pd system is not sufficiently stable to preserve the hydrogen in the crystal lattice at RT and is only suitable for hydrogen sensor development. Additionally, the high cost and low production of Pd make it unfavorable for industrial applications. Mg, by contrast, is a promising candidate for potential H_2 storage materials because of the high stability and hydrogen content of MgH_2.[20−22] Hydrogen can be stably stored in MgH_2 at RT. Mg is a low-cost and low-weight material.[23] However, the hydrogenation of Mg is challenging, requiring high temperatures (at least above 600 K) and a high-pressure hydrogen environment.[24−26] Pd and Mg were both used in this experiment because they serve different functions. Mg is an attractive candidate for hydrogen storage at RT. Meanwhile, Pd is a highly efficient catalyst for hydrogen dissociation. When a Pd capping layer is added to Mg, the RT-formation of MgH_2 is possible with just 1 bar of H_2 gas. In this study, we examined an alternative approach that involved capping Pd on Mg to facilitate hydrogen diffusion into Mg at RT at 1 bar hydrogen pressure. Through careful comparison of samples before and after H_2 exposure, the hydrogenation of Mg and its influence on the magnetic properties, such as H_c modification and spin-dependent transport properties, of a Pd/Co/Mg/Fe device were investigated.

EXPERIMENTAL METHOD

The Pd(5 nm)/Co(3 nm)/Mg(25 nm)/Fe(10 nm) multilayer sample, as shown in Figure 1a, was deposited on c-sapphire $Al_2O_3(0001)$ substrates at RT through e-beam evaporation under ultrahigh vacuum at 5×10^{-9} mbar. The bottom electrode (Fe) and the top electrode (Pd/Co/Mg) were patterned into a 200 × 3000 μm stripe through shadow masking, and the top Pd capping layer protected the

Received: March 16, 2023
Accepted: June 27, 2023
Published: July 17, 2023

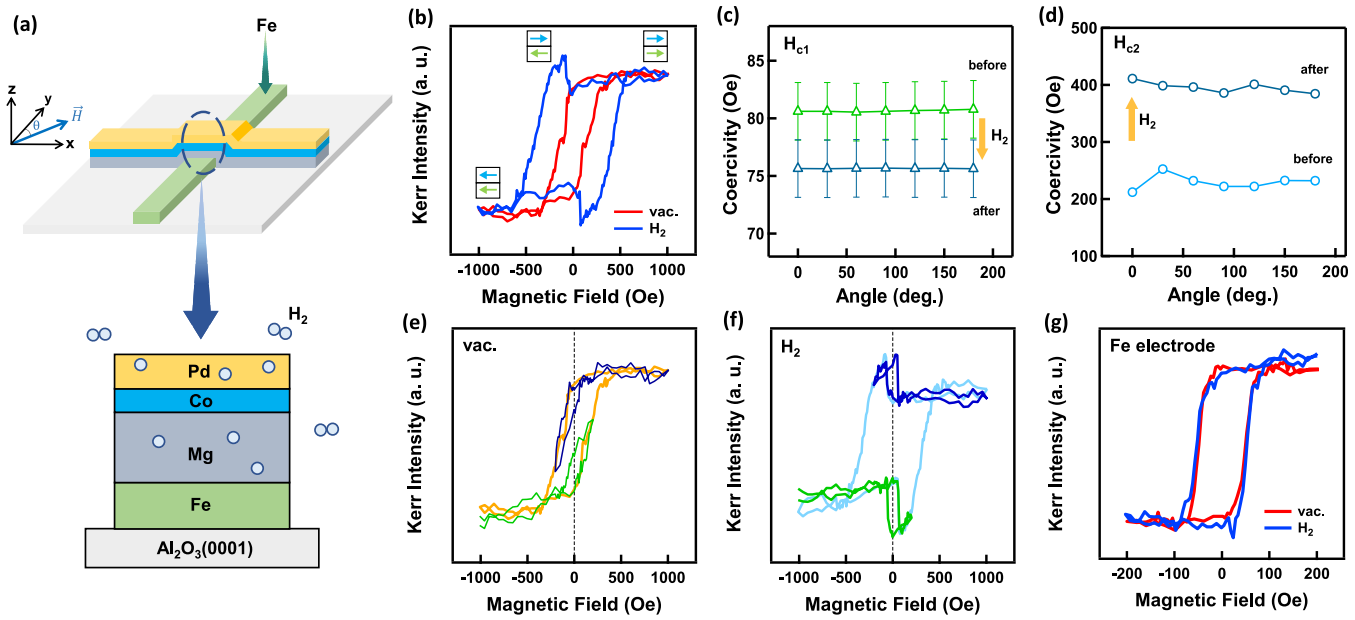

Figure 1. (a) Schematic of the cross-bar patterned structure (upper) and enlarged junction area (lower) showing a layer sequence of the Pd(5 nm)/Co(3 nm)/Mg(25 nm)/Fe(10 nm) sample geometry on exposure to H_2 gas at RT. (b) MOKE hysteresis loops in vacuum and a H_2 environment. (c, d) Dependence of coercivity of Fe (H_{c1}) and Co (H_{c2}) at various magnetic field orientations upon exposure to H_2. (e, f) Minor MOKE hysteresis loops before and after hydrogenation. (g) Hysteresis of the Fe electrode after exposure to 1 bar H_2 gas.

underlayers from oxidation and catalyzed the absorbed H_2 into hydrogen atoms for further diffusion to the Mg layer.

In this study, the hydrogenation of Pd/Co/Mg/Fe is achieved by direct exposure to H_2 gas under the gas pressure of 1 bar at RT in a chamber, which is pre-vacuumed to a base pressure of 5×10^{-5} mbar. The magnetic properties were characterized using the longitudinal magneto-optical Kerr effect (L-MOKE) at a base pressure of 5×10^{-5} mbar and 1 bar H_2, respectively. In-plane (IP) hysteresis loops were measured using vibrating sample magnetometry (VSM) at atmospheric pressure before and after hydrogenation to further verify the magnetic properties of the hydride sample. The thin-film structure was characterized using X-ray diffraction (XRD) to verify the effects of hydrogeneration. MR was measured using a four-probe measurement with a current source (Keithley 2400) and voltage meter (Keithley 2000) in ambient conditions with and without 1 bar H_2 exposure under an external IP magnetic field to reveal the influence of hydrogeneration on the sample's magneto-transport properties.

EXPERIMENTAL RESULTS

A schematic of the sample geometry (upper figure) and enlarged layer structure with hydrogen gas exposure (lower figure) is shown in Figure 1a. The top Pd layer dissociated H_2 molecules into H atoms on its surface and facilitated the diffusion of H atoms through the Co interlayer to the Mg layer, which lowered the temperature and pressure required for H absorption to form Mg hydride.[27] The red and blue curves shown in Figure 1b indicate the hysteresis loops measured at the junction area using L-MOKE in a vacuum and a H_2 environment, in which typical two-step pseudo-spin valve behavior was observed; however, the hysteresis loops measured in a vacuum (red curve) demonstrated a small window of antiparallel (AP) magnetization alignment of the two ferromagnets (FMs). By contrast, the hydrogenated sample exhibited a broadened AP state indicated by the AP blue and light green arrows shown in Figure 1b. The suddenly enhanced Kerr intensity may be attributable to the Kerr rotation angle.[28,29] The variation in coercivity of Fe (H_{c1}) and Co (H_{c2}) as a function of the angle to the applied magnetic field, where theta = 0° is along the Fe electrode, is shown in Figure 1c,d. After exposure to H_2 gas, H_{c1} decreased from 80.5 to 75.5 Oe, whereas H_{c2} exhibited an opposite trend, increasing from 229 to 395 Oe. The lower H_{c1} and higher H_{c2} values could be easily distinguished because Fe was the soft ferromagnet and Co was the hard ferromagnet.[31] Because the orientation of the deposition source was parallel (P) to the Al_2O_3(0001) substrate and the angular independent H_c, as shown in Figure 1c,d, the junction of the Pd/Co/Mg/Fe multilayer sample was magnetically isotropic.

A stable AP configuration window of magnetization of the two FM layers is crucial for device application which is attributed to magnetic memory devices' writing and reading the data. Therefore, a minor loop measurement was importantly performed to examine the AP stability of the samples before and after hydrogenation. In Figure 1e,f, the yellow and light blue lines exhibit the major loops that correspond to the vacuum and hydrogenation curves shown in Figure 1b. In Figure 1e,f, the dark blue and green curves represent the field alternating between positive and negative magnetic saturation fields, respectively. The magnetic field range for the dark blue and green minor loops in Figure 1e,f extends from 1000 to −200 Oe and from −1000 to 200 Oe, respectively. As shown in Figure 1e,f, the minor loop of the sample measured under H_2 exposure revealed a more symmetric and stable AP configuration that was more favorable for device application. To further identify the effect of hydrogenation on the magnetic properties of the FM layer, we also measured the H_c variation on the bottom Fe electrode without the Mg, Co, and Pd capping layer, as shown in Figure 1g. The MOKE results demonstrated that H_c remained constant before and after H_2 exposure. We propose that the

https://doi.org/10.1021/acsomega.3c01778
ACS Omega 2023, 8, 26948−26954

hydrogen diffused from the Pd layer to the Mg layer between the Co and Fe layers, converting Mg to MgH_2. Therefore, the Mg hydride in the Pd/Co/Mg/Fe system not only stored H_2 but also affected the top and bottom magnetic layers.

The way to determine H_c is to take the Kerr intensity corresponding to the positive (I_{+s}) and negative (I_{-s}) saturation magnetization of the hysteresis curve. We obtain the average Kerr intensity $I_{Hc} = (I_{+s} + I_{-s})/2$. Then the external field H_{ex} corresponding to the I_{Hc} value is identified as the coercive field H_c. For example, the positive and negative saturation magnetic field chosen for the determination of H_{c1} is around +1000 and −132 Oe, as shown in Figure 1c. The chosen saturation field for H_{c2} is approximately −132 and −1000 Oe, as shown in Figure 1d. Accordingly, I_{+s}, I_{-s}, and I_{Hc}, as well as H_c, are sequentially determined. After the hydrogenation effect, the saturation magnetic field chosen for H_{c1} is around 1000 and −80 Oe, as shown in Figure 1c; the chosen saturation field for H_{c2} is approximately −80 and −1000 Oe, as shown in Figure 1d, respectively. For the detailed analysis, the error bars are added in Figure 1c,d. The error bars in Figure 1c represent the uncertainties in the values of the applied magnetic field. The hysteresis loop measurements were conducted at a field interval of 5 Oe, and the error bar represents the range of ±2.5 Oe around the median value. Similarly, in Figure 1d, the hysteresis loops were measured at a field interval of 10 Oe, resulting in the uncertainty of a magnetic field value of ±5 Oe. In Figure 1d, the error bars are smaller than the data markers, indicating a relatively small level of uncertainty as compared to H_{c2}. This also allows for clear observation and analysis of the changes in H_{c2}. On the other hand, the H_{c1} change shown in Figure 1b is tiny to observe after the hydrogenation. Although the change in H_{c1} is close to the error bar in Figure 1c, all of the data points show the consistent 5 Oe-reduction after hydrogenation. In contrast to Figure 1c measured in the junction area, the invariant H_c in Figure 1g is straightforward because it is measured from a bare Fe electrode without a Pd covering, on which there should be no hydrogenation effect.

In addition to the proposed decoupling effect induced by MgH_2 between the Co and Fe layers, a potential factor contributing to the observed change in the Hc_2 of Co, as depicted in Figure 1d, could be attributed to the hydrogenation effect at the Co/Mg interface. This effect may arise from various factors, such as the potential formation of hydrides within the interfacial Co-Mg alloy or the structural and electrical proximity between Co and MgH_2 at the interface. The simultaneous impact of MgH_2-induced magnetic decoupling and interfacial proximity effect in Co/MgH_2 on modulating the Hc of Co poses a challenge in confirming their individual contributions.

The hysteresis loops measured using IP MOKE and VSM in air after H_2 absorption are shown in Figure 2a,b. Because the MOKE intensity depends heavily on the relative orientation of the magnetization of magnetic layers and the polarization of light,[32] the hysteresis loops responded qualitatively to the changes in magnetization. To further understand why the MOKE hysteresis curve demonstrated a higher Kerr intensity of the Fe layer after hydrogenation, VSM analysis was conducted to quantitatively illustrate the magnetic behaviors of the Pd/Co/Mg/Fe multilayer. The cycling of MOKE intensity with the applied magnetic field is shown in Figure 2a. The hysteresis loop displayed typical spin valve-type characteristics at RT. As the magnetic field swept from a positive field to

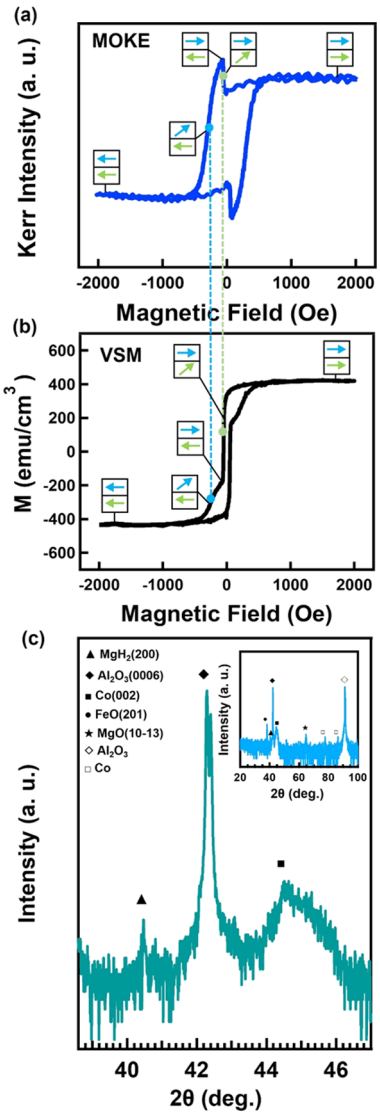

Figure 2. (a, b) MOKE and VSM hysteresis loops of the sample in air after absorbing 1 bar H_2 gas at RT. (c) XRD pattern of the sample after hydrogenation, indicating MgH_2 formation. The inset displays the wide-range XRD pattern, highlighting the discernible peaks.

the H_{c1} value, for example, from 1000 to −70 Oe, the MOKE intensity remained almost constant when the magnetizations of the FM electrodes were P. When the magnetic field exceeded −70 Oe, the magnetization of the Fe layer changed, causing higher MOKE intensity because of the AP configuration of the Fe and Co layers. With further sweeping of the magnetic field from $-H_{c2}$ to the negative magnetic saturation, the MOKE intensity decreased until the magnetization of the two magnetic layers was aligned (blue and light green arrows).

In our previous study, the CoPd alloy thin-film exhibited a Kerr intensity decrease by hydrogenation.[28] Considerable changes in the magneto-optical properties were observed. Correspondingly, the Kerr hysteresis loops considerably changed as well. Moreover, the hydrogenation effect on the Kerr signal is also obtained in the Pd/Fe bilayer.[29] The extinction angle was shifted after hydrogenation, indicating the variation of Kerr rotation. These changes result in the change of Kerr intensity and the possible reversion of the Kerr hysteresis loop, if the shift of the extinction angle is large enough. In Luo et al.'s study on Co/Pd(110), the Kerr

https://doi.org/10.1021/acsomega.3c01778
ACS Omega 2023, 8, 26948−26954

hysteresis loops are reversed below 2.7 ML with respect to those of thicker Co films.[30] This is attributed to the mixture of the negative Kerr rotation from the Co/Pd interface and the positive polar Kerr rotation from the non-interface part of the Co film.[30] Their observation and discussion imply that the hydrogenation process could very possibly change the optical properties of the multilayers and result in the reversion of Kerr signals. Figure S1 in the Supporting Information illustrates the possible mechanisms in the Kerr signal revision. The diagrams in Figure S1a show the initial state of Fe and Co layers. The parabolic curves represent the detected light intensity plotted as a function of the analyzer angle φ under positive and negative saturation ($+M_s$ and $-M_s$). The dashed line indicates a possibly chosen analyzer angle in the measurement of the Kerr hysteresis loop. When the analyzer angle is fixed and the magnetic field is scanned, one can measure the intensity difference between $+M_s$ and $-M_s$, as indicated by a triangle and square, respectively. This intensity difference corresponds to the Kerr signal in the hysteresis loop, as displayed in the insets. Through the superposition of the Kerr signal from Fe and Co, the entire hysteresis loop shows the normal two-step switching. The diagrams in Figure S1b illustrate the possible conditions of Fe and Co layers after hydrogenation. The parabola curves of Co may shift and the Kerr rotation may reverse, like the observation of Luo et al.[30] As a result of the Kerr signal reversion, the bottom Fe layer could reveal the inversed hysteresis loop. Accordingly, the entire hysteresis loop by superposition of Fe and Co could exhibit the anomalous two-step switching behavior, as shown in the bottom of Figure S1b, similar to the measurement result shown in Figure 2a.

VSM measurements of the quantity of the magnetization variation of the Pd/Co/Mg/Fe multilayer as a function of the magnetic field after H_2 absorption and the blue and light green arrows corresponding to the magnetization direction are clearly shown in Figure 2b. Magnetization decreased from approximately 400 to −200 emu/cm^3 during the reversal of the field at the H_{c1} value, which corresponded with the magnetization reversal of the thicker 10 nm Fe layer; the change from −200 to −400 emu/cm^3 indirectly demonstrated the second magnetization reversal of the thinner 3 nm Co layer. The hysteresis loop measured using VSM (Figure 2b) demonstrates the layer-related MOKE intensity variation shown in Figure 2a. The green and blue dashed lines indicate H_{c1} and H_{c2}, demonstrating the Kerr intensity increase due to the change in the Kerr rotation angle corresponding to the AP alignment of magnetization between Fe and Co, which illustrates the extended AP states caused by hydrogenation, as shown in Figure 1.

Figure 1g shows that the H_c of Fe is around 50 (Oe), regardless of whether it is in a thin-film-type or a device-type sample. This indicates that in Figure 1, the small H_c (<100 Oe) belongs to the Fe layer and the large H_c (>200 Oe) belongs to the Co layer. Furthermore, based on the VSM hysteresis loop for the Pd/3 nm Co/Mg/10 nm Fe structure, as shown in Figure 2b, the magnetic moment of the small H_c is more than three times that of the large H_c. Considering that the Fe and Co thicknesses are 10 and 3 nm, respectively, it is reasonable to conclude that the significant signal drop during M-reversion with a small H_c can be attributed to the Fe layer.

To explore the effect of hydrogen on the structure of the multilayer thin films, XRD analysis was undertaken. The inset of the XRD results displays a wider range and reveals additional elements present in the device. The presence of the Fe layer influences the growth structure of the upper Mg layer, leading to the formation of an amorphous phase. Consequently, the XRD data did not indicate evidence of crystalline Mg in the device. The XRD results of the hydrogenate sample, where the peaks at 40.3, 41.8, and 44.5° represent the MgH_2(002), Al_2O_3(0006), and Co(002) phases, respectively, are presented in Figure 2c. No pure Mg peak was recorded after 1 bar hydrogen exposure, which is consistent with previous studies and indicates that the hydrogen exposure caused hydrogenation of the Mg layer.[33] Moreover, MgH_2 was detected in the sample stored in a chamber with a base pressure of 5×10^{-5} mbar after 2 months, indicating that Mg can effectively be used to store hydrogen at RT for a long duration. Studies have demonstrated that hydrogenation affects the optical properties of some hydride materials such as MgH_2.[34−36]

In the previously reported XRD data of hydrogenated Pd/Co/Mg/Al_2O_3(0001),[33] initially the pure Mg(0004) peak at 34.4° was visible. After hydrogenation, the Mg(0004) peak disappeared and was replaced by the MgH_2(200) phase at 40.3°. In the investigation of the present sample Pd/Co/Mg/10-nm Fe/Al_2O_3(0001), the presence of the bottom Fe layer influences the growth structure of the upper Mg layer, leading to the formation of an amorphous phase. Consequently, the XRD data does not show any observable crystalline feature of Mg. Correspondingly, the intensity of the MgH_2(200) peak formed is weaker, as compared to the previous data of Pd/Co/Mg/Al_2O_3(0001), possibly because of the presence of the amorphous Mg layer.

DISCUSSION

MOKE, VSM, and XRD analysis confirmed the hydrogenation of the multilayer structure through characterization of the hysteresis loops and the crystalline structure. This transport behavior has considerable application potential because the structure of the Pd(5 nm)/Co(3 nm)/Mg(25 nm)/Fe(10 nm) multilayer is identical to that of pseudo-spin valve devices. Figure 3 presents the measured magneto-transport properties, illustrating the resistance response to the applied magnetic field. In Figure 3a, the pseudo-spin valve was constructed with

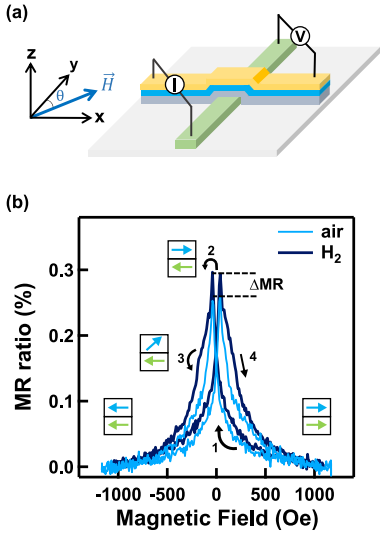

Figure 3. (a) Schematic of the MR measurement configuration. (b) MR curve before and after hydrogenation of the multilayer sample.

https://doi.org/10.1021/acsomega.3c01778
ACS Omega 2023, 8, 26948−26954

the hydrogenated Mg spacer sandwiched between two perpendicular ferromagnetic electrodes, in which Fe served as the soft FM layer and the Co layer above served as the hard layer. The MR characteristics were measured in the current-perpendicular-to-the-plane configuration using the four-probe method with a bias voltage applied on the top electrode and the bottom electrode grounded.

The hydrogenation effect on the Pd/Co/Mg/Fe multilayer structure was further demonstrated by its MR before and after the exposure to 1 bar H_2. The samples were all measured under ambient conditions. The resistance curves demonstrate the typical pseudo-spin valve-type characteristics with a magnetoresistive ratio defined as

$$\mathrm{MR}\% = \frac{\Delta R}{R_\mathrm{P}} \times 100\% = \frac{R_\mathrm{AP} - R_\mathrm{P}}{R_\mathrm{P}} \times 100\% \quad (1)$$

where R_P and R_AP represent the resistances with the magnetizations of the two FM electrodes in the P and AP configurations, respectively.

The MR loop of the sample is shown in Figure 3b, exhibiting typical pseudo-spin valve characteristics both in air (blue curve) and after H_2 absorption (solid black curve). Both MR measurements are finished in the air. The magnetic field was swept between 1000 and −1000 Oe, with the blue and light green arrows in the figure indicating the direction of the magnetization flipping. The numbers on the blue arrows indicate the measurement sequence of the MR curve. When the field decreased gradually from 1000 across the zero field, the magnetization of two FM layers remained P. The resistance increased with the decreasing field, demonstrating that the magnetization of part of the Fe domain was changing direction, which caused higher scattering probability for the spin-polarized electron transport from the Co layer to the Fe layer, and therefore, the resistance increased. While the field continued sweeping to the negative, crossing the H_{c1} value, the magnetization of Fe switched along the field direction to the opposite direction of the magnetization of the Co layer, causing an AP state. The resistance reached its highest value as the direction of the magnetization of Fe entirely switched to the opposite of that of Co in the AP state. Subsequently, the resistance decreased with increasing field until the direction of magnetization of Co completely switched to the field direction at −1000 Oe, reconstituting the P state. During the positive field sweeping, the magnetization underwent the same process, causing a symmetrical MR loop.

Demonstrating the effect of hydrogenation on the sample, the MR curve was clearly broader after hydrogenation than in air. The MR ratio also increased by 36% from 0.22 ± 0.01% (air) to 0.30 ± 0.01% (H_2). The MR curve of the pseudo-spin valve with the hydrogenated MgH_2 spacer exhibited a broadened loop (step number 3). This may be attributable to the enhancement and reduction of the coercivity of Co and Fe, respectively, which is consistent with the MOKE results shown in Figure 2.

According to the previous reports, magnesium hydride has a high volumetric density of 1.58 g/cm^3 and a volumetric hydrogen density of 0.11 g/cm^3.[26,37] The formation of MgH_2 is also detected by the XRD analysis. More importantly, the increase in resistance is attributed to the formation of MgH_2 at the interface between Pd and Mg.[38] Based on the aforementioned results, we hypothesize that the formation of MgH_2 and its high hydrogen capacity in the device increase the spin scattering probability during the flow of electrons through the junction, which enhances the MR ratio. Furthermore, the MR curve in Figure 3 exhibits two significant changes: an increase in the MR ratio and a broadening of the MR curve. The presence of MgH_2 at the interface has been verified through XRD analysis, suggesting a potential augmentation in the spin scattering probability and subsequent enhancement of the MR ratio.[38] Besides, the broadening of the MR curve is probably attributed to the CoMg-H formation at the interface between Co and Mg layers. The interfacial effect substantially heightened the H_c of the Co layer, resulting in a distinctly well-defined AP state within the spin valve. Consequently, this may also lead to an augmented MR ratio.

Additionally, in an ambient environment, the MR ratio of the Pd/Co/Mg/Fe multilayer device increased after the absorption of H_2, indirectly demonstrating that hydrogen could be stably stored in Mg in the form of MgH_2. The high stability and high hydrogen storage capability of MgH_2 make the Mg-based pseudo-spin valve favorable for device application.

In contrast to the hydrogenation effect, it is also interesting to investigate the dehydrogenation effect on magnetism. However, the desorption of hydrogen from MgH_2 requires high-temperature annealing at least above 600 K,[24,26] which could potentially alter or even damage the magnetic multilayer device of Co/Mg/Fe. Additionally, the annealing process can lead to more interlayer diffusion and alloy formation, further complicating the situation. As a result, the desorption effect is inevitably coupled with a more severe annealing effect, resulting in a complex situation. Therefore, investigation of the dehydrogenation effect is not suitable for this system. Instead, the voltage or current-driven migration of hydrogen will be carried out in the future work. This could potentially alter the hydrogen distribution and the device properties.

CONCLUSIONS

In summary, the magnetic properties, crystal structure, and MR in a Pd/Co/Mg/Fe multilayer were examined to study the effect of hydrogenation on interlayer coupling and magneto-transport properties using L-MOKE, VSM, and a four-probe analysis. The results indicate that the process of hydrogenation can effectively enhance the H_c of the Co layer and, in turn, decrease the H_c of the Fe layer, with the formation of MgH_2. This broadens the AP window for device applications. Accordingly, the MR ratio increased from 0.22 ± 0.01 to 0.30 ± 0.01%, which also suggests that MgH_2 may have increased spin scattering probability, helping to preserve spin-dependent transport properties. This study revealed a significant pathway toward applying hydrogenation in spintronic devices.

ASSOCIATED CONTENT

Supporting Information

The Supporting Information is available free of charge at https://pubs.acs.org/doi/10.1021/acsomega.3c01778.

Figure S1 Schematic illustrations to demonstrate how hydrogen affects the Kerr intensity and MOKE hysteresis loop; Figure S2: Optical image of the junction area of the Pd/Co/Mg/Fe heterostructure on Al2O3(0001), and AFM images taken before and after hydrogenation (PDF)

https://doi.org/10.1021/acsomega.3c01778
ACS Omega 2023, 8, 26948−26954

AUTHOR INFORMATION

Corresponding Authors

Jhen-Yong Hong − *Department of Physics, Tamkang University, New Taipei City 251301, Taiwan*; Email: jyhong@mail.tku.edu.tw

Wen-Chin Lin − *Department of Physics, National Taiwan Normal University, Taipei 11677, Taiwan*; orcid.org/0000-0002-1457-8968; Email: wclin@ntnu.edu.tw

Authors

Li-Jie Liaw − *Department of Physics, National Taiwan Normal University, Taipei 11677, Taiwan*; orcid.org/0000-0002-9077-7686

Zi-Qi Liu − *Department of Physics, National Taiwan Normal University, Taipei 11677, Taiwan*

Po-Wei Chen − *Department of Physics, National Taiwan Normal University, Taipei 11677, Taiwan*

Shi-Yu Liu − *Department of Physics, National Taiwan Normal University, Taipei 11677, Taiwan*

Alltrin Dhanarajagopal − *Department of Physics, National Taiwan Normal University, Taipei 11677, Taiwan*

Fang-Yuh Lo − *Department of Physics, National Taiwan Normal University, Taipei 11677, Taiwan*

Complete contact information is available at: https://pubs.acs.org/10.1021/acsomega.3c01778

Notes

The authors declare no competing financial interest.

ACKNOWLEDGMENTS

This study was financially sponsored by the Ministry of Science and Technology of Taiwan under Grant nos. MOST 111-2112-M-003-012, MOST 111-2124-M-003-002, MOST 111-2923-M-003-001-MY3, and MOST 111-2112-M-003-013.

REFERENCES

(1) Pinarbasi, M.; Kent, A. D. Perspectives on Spintronics Technology Development: Giant Magnetoresistance to Spin Transfer Torque Magnetic Random Access Memory. *APL Mater.* **2022**, *10*, No. 020901.

(2) Faure-Vincent, J.; Tiusan, C.; Jouguelet, E.; Canet, F.; Sajieddine, M.; Bellouard, C.; Popova, E.; Hehn, M.; Montaigne, F.; Schuhl, A. High Tunnel Magnetoresistance in Epitaxial Fe/MgO/Fe Tunnel Junctions. *Appl. Phys. Lett.* **2003**, *82*, 4507−4509.

(3) Parkin, S. S. P.; Kaiser, C.; Panchula, A.; Rice, P. M.; Hughes, B.; Samant, M.; Yang, S. H. Giant Tunnelling Magnetoresistance at Room Temperature with MgO (100) Tunnel Barriers. *Nat. Mater.* **2004**, *3*, 862−867.

(4) Willing, S.; Schlage, K.; Bocklage, L.; Ramin Moayed, M. M.; Gurieva, T.; Meier, G.; Röhlsberger, R. Novel Tunnel Magneto-resistive Sensor Functionalities via Oblique-Incidence Deposition. *ACS Appl. Mater. Interfaces* **2021**, *13*, 32343−32351.

(5) Tudu, B.; Tiwari, A. Recent Developments in Perpendicular Magnetic Anisotropy Thin Films for Data Storage Applications. *Vacuum* **2017**, *146*, 329−341.

(6) Yang, S.; Zhang, J. Current Progress of Magnetoresistance Sensors. *Chemosensors* **2021**, *9*, 211.

(7) Rizal, C.; Moa, B.; Niraula, B. B. Ferromagnetic Multilayers: Magnetoresistance, Magnetic Anisotropy, and Beyond. *Magneto-chemistry* **2016**, *2*, 22.

(8) Djamal, M.; Ramli, R.; Khaiurrijal, K. Giant Magnetoresistance Material and Its Potential for Biosensor Applications. In *International Conference on Instrumentation, Communication, Information Technology, and Biomedical Engineering*, 23−25 November, 2009.

(9) Parks, D. C.; Chen, P. J.; Egelhoff, W. F.; Gomez, R. D. Interfacial Roughness Effects on Interlayer Coupling in Spin Valves Grown on Different Seed Layers. *J. Appl. Phys.* **2000**, *87*, 3023−3026.

(10) Chang, P. C.; Chen, Y. C.; Hsu, C. C.; Mudinepalli, V. R.; Chiu, H. C.; Lin, W. C. Hydrogenation-Induced Reversible Spin Reorientation Transition in Co50Pd50 Alloy Thin Films. *J. Alloys Compd.* **2017**, *710*, 37−46.

(11) Chang, P. C.; Chuang, T. H.; Wei, D. H.; Lin, W. C. Thermally Modulated Hydrogenation in FexPd1-x Alloy Films: Temperature-Driven Peculiar Variation of Magnetism. *Appl. Phys. Lett.* **2020**, *116*, 102407.

(12) Chang, P. C.; Liu, C. M.; Hsu, C. C.; Lin, W. C. Hydrogen-Mediated Magnetic Domain Formation and Domain Wall Motion in Co30Pd70 Alloy Films. *Sci. Rep.* **2018**, *8*, 6656.

(13) Munbodh, K.; Perez, F. A.; Keenan, C.; Lederman, D.; Zhernenkov, M.; Fitzsimmons, M. R. Effects of Hydrogen/Deuterium Absorption on the Magnetic Properties of Co/Pd Multilayers. *Phys. Rev. B - Condens. Matter Mater. Phys.* **2011**, *83*, No. 094432.

(14) Adams, B. D.; Chen, A. The Role of Palladium in a Hydrogen Economy. *Mater. Today* **2011**, *14*, 282−289.

(15) Bordoloi, A. K.; Auluck, S. Electronic Structure of Palladium. *Phys. Rev. B* **1983**, *27*, 5116−5118.

(16) Lewis, F. A. The Palladium-Hydrogen System. *Platinum Met. Rev.* **1982**, *26*, 20−27.

(17) Liang, J. Y.; Pai, Y. C.; Lam, T. N.; Lin, W. C.; Chan, T. S.; Lai, C. H.; Tseng, Y. C. Using Magnetic Structure of Co40Pd60/Cu for the Sensing of Hydrogen. *Appl. Phys. Lett.* **2017**, *111*, No. 023503.

(18) Causer, G. L.; Kostylev, M.; Cortie, D. L.; Lueng, C.; Callori, S. J.; Wang, X. L.; Klose, F. In Operando Study of the Hydrogen-Induced Switching of Magnetic Anisotropy at the Co/Pd Interface for Magnetic Hydrogen Gas Sensing. *ACS Appl. Mater. Interfaces* **2019**, *11*, 35420−35428.

(19) Akamaru, S.; Matsumoto, T.; Murai, M.; Nishimura, K.; Hara, M.; Matsuyama, M. Sensing Hydrogen in the Gas Phase Using Ferromagnetic Pd-Co Films. *J. Alloys Compd.* **2015**, *645*, S213−S216.

(20) Green, M.; VanTran, A. T.; Smedley, R.; Roach, A.; Murowchick, J.; Chen, X. Microwave Absorption of Magnesium/Hydrogen-Treated Titanium Dioxide Nanoparticles. *Nano Mater. Sci.* **2019**, *1*, 48−59.

(21) Ouyang, L.; Liu, F.; Wang, H.; Liu, J.; Yang, X. S.; Sun, L.; Zhu, M. Magnesium-Based Hydrogen Storage Compounds: A Review. *J. Alloys Compd.* **2020**, *832*, No. 154865.

(22) Matysina, Z. A.; Gavrylyuk, N. A.; Kartel, M.; Veziroglu, A.; Veziroglu, T. N.; Pomytkin, A. P.; Schur, D. V.; Ramazanov, T. S.; Gabdullin, M. T.; Zolotarenko, A. D.; Zolotarenko, A. D.; Shvachko, N. A. Hydrogen Sorption Properties of New Magnesium Intermetallic Compounds with MgSnCu4 Type Structure. *Int. J. Hydrogen Energy* **2021**, *46*, 25520−25532.

(23) Kumar, A.; Kumar, S.; Mukhopadhyay, N. K. Introduction to Magnesium Alloy Processing Technology and Development of Low-Cost Stir Casting Process for Magnesium Alloy and Its Composites. *J. Magnes. Alloys.* **2018**, *6*, 245−254.

(24) Lin, Q.; Yang, X.; Lin, J.; Guo, Z.; He, Y. The Structure and Magnetic Properties of Magnesium-Substituted LaFeO3 Perovskite Negative Electrode Material by Citrate Sol-Gel. *Int. J. Hydrogen Energy* **2018**, *43*, 12720−12729.

(25) Feng, D.; Zhou, D.; Zhao, Z.; Zhai, T.; Yuan, Z.; Sun, H.; Ren, H.; Zhang, Y. Progress of Graphene and Loaded Transition Metals on Mg-Based Hydrogen Storage Alloys. *Int. J. Hydrogen Energy* **2021**, *46*, 33468−33485.

(26) Yartys, V. A.; Lototskyy, M. V.; Akiba, E.; Albert, R.; Antonov, V. E.; Ares, J. R.; Baricco, M.; Bourgeois, N.; Buckley, C. E.; Bellosta von Colbe, J. M.; Crivello, J. C.; Cuevas, F.; Denys, R. V.; Dornheim, M.; Felderhoff, M.; Grant, D. M.; Hauback, B. C.; Humphries, T. D.; Jacob, I.; Jensen, T. R.; deJongh, P. E.; Joubert, J. M.; Kuzovnikov, M. A.; Latroche, M.; Paskevicius, M.; Pasquini, L.; Popilevsky, L.; Skripnyuk, V. M.; Rabkin, E.; Sofianos, M. V.; Stuart, A.; Walker, G.; Wang, H.; Webb, C. J.; Zhu, M. Magnesium Based Materials for

Hydrogen Based Energy Storage: Past, Present and Future. *Int. J. Hydrogen Energy* **2019**, *44*, 7809−7859.
(27) Schlapbach, L.; Züttel, A. Hydrogen-storage materials for mobile applications. *Nature* **2001**, *414*, 353−358.
(28) Lin, W. C.; Tsai, C. J.; Huang, H. Y.; Wang, B. Y.; Mudinepalli, V. R.; Chiu, H. C. Hydrogen-Mediated Long-Range Magnetic Ordering in Pd-Rich Alloy Film. *Appl. Phys. Lett.* **2015**, *106*, No. 012404.
(29) Lin, W. C.; Chi, C. S.; Ho, T. Y.; Tsai, C. J. Hydrogen Absorption Induced Reversible Effect on Magneto-Optical Property of Pd/Fe, Pd/Co and Pd/Ni Bilayers. *Thin Solid Films* **2013**, *531*, 487−490.
(30) Luo, F.; Yan, L.; Przybylski, M.; Shi, Y.; Kirschner, J. Unusual temperature dependence of polar Kerr rotation in ultrathin Co films grown on Pd(110). *J. Magn. Magn. Mater.* **2007**, *316*, e342−e345.
(31) Prieto-Ruiz, J. P.; Miralles, S. G.; Großmann, N.; Aeschlimann, M.; Cinchetti, M.; Prima-García, H.; Coronado, E. Design of Molecular Spintronics Devices Containing Molybdenum Oxide as Hole Injection Layer. *Adv. Electron. Mater.* **2017**, *3*, No. 1600366.
(32) Arregi, J. A.; Riego, P.; Berger, A. What Is the Longitudinal Magneto-Optical Kerr Effect? *J. Phys. D Appl. Phys.* **2017**, *50*, No. 03LT01.
(33) Liaw, L. J.; Chang, P. C.; Chen, P. W.; Liu, Z. Q.; Liu, S. Y.; Hsieh, C. T.; Dhanarajgopal, A.; Chern, M. Y.; Lo, F. Y.; Lin, W. C. Hydrogen-Induced Magnetic and Structural Changes in Pd/Co/Mg Multilayer. *Surf. Interfaces* **2023**, *36*, No. 102503.
(34) Richardson, T. J.; Slack, J. L.; Armitage, R. D.; Kostecki, R.; Farangis, B.; Rubin, M. D. Switchable Mirrors Based on Nickel-Magnesium Films. *Appl. Phys. Lett.* **2001**, *78*, 3047−3049.
(35) Nagengast, D. G.; VanGogh, A. T. M.; Kooij, E. S.; Dam, B.; Griessen, R. Contrast Enhancement of Rare-Earth Switchable Mirrors through Microscopic Shutter Effect. *Appl. Phys. Lett.* **1999**, *75*, 2050−2052.
(36) Yamada, Y.; Bao, S.; Tajima, K.; Okada, M.; Yoshimura, K. Optical Properties of Switchable Mirrors Based on Magnesium-Calcium Alloy Thin Films. *Appl. Phys. Lett.* **2009**, *94*, 191910.
(37) Kajiwara, K.; Sugime, H.; Noda, S.; Hanada, N. Fast and Stable Hydrogen Storage in the Porous Composite of MgH2 with Nb2O5 Catalyst and Carbon Nanotube. *J. Alloys Compd.* **2022**, *893*, No. 162206.
(38) Hadjixenophontos, E.; Zhang, K.; Weigel, A.; Stender, P.; Schmitz, G. Hydrogenation of Pd/Mg Films: A Quantitative Assessment of Transport Coefficients. *Int. J. Hydrogen Energy* **2019**, *44*, 27862−27875.

https://doi.org/10.1021/acsomega.3c01778
ACS Omega 2023, 8, 26948−26954